

Adaptive optics sensing and control technique to optimize the resonance of the Laguerre-Gauss 33 mode in Fabry-Perot cavities

G. Vajente*

Istituto Nazionale di Fisica Nucleare sezione di Pisa, 56127 Pisa (PI), Italy

R. A. Day

European Gravitational Observatory, 56021 Cascina (PI), Italy

(Received 9 May 2013; published 24 June 2013)

Second and third generation gravitational wave interferometric detectors will be limited in their sensitivity by thermal noise of the core optics. One way to reduce this contribution is to use an input laser beam with a more uniform distribution of the power: for this reason the use of the Laguerre-Gauss $LG_{3,3}$ mode as interferometer input has been suggested. The main issue with this approach is the fact that in resonant cavities with spherical mirrors the input mode will be degenerate with nine other modes. This implies very stringent requirements on the mirror surface quality, beyond the present polishing technology capabilities: it is not possible to obtain mirrors with low enough surface roughness to meet the requirements for the operation of a gravitational wave detector. In a previous paper an approach to apply in situ thermal corrections to the main surface of the mirrors was proposed. In this paper we develop further the technique, showing that it is possible to compute the optimal correction using only the information that can be extracted from the intensity images in reflection of the resonant cavity, without any *a priori* knowledge of the mirror surface maps. We test our proposal using optical simulations and we are able to considerably improve the quality of the beam reflected from a cavity with realistic mirror surface maps: without any correction the purity of the reflected beam was degraded to below 90%; with the proposed adaptive optics system we could recover a purity of 99.96%. The implementation of the proposed system would allow the use of a $LG_{3,3}$ input mode with the mirror qualities available today. In addition we show that it is possible to correct the aberrations introduced by both mirrors acting only on one of the two. In this way it is possible to avoid introducing unwanted thermal lensing in the input mirrors.

DOI: [10.1103/PhysRevD.87.122005](https://doi.org/10.1103/PhysRevD.87.122005)

PACS numbers: 04.80.Nn, 07.60.Ly, 95.55.Ym

I. INTRODUCTION

Advanced [1–3] and third generation [4] gravitational wave detectors will use long baseline resonant cavities, in a Michelson configuration, to monitor the distance variation between test masses, composed of high quality mirrors. Any spurious motion of the surfaces will mimic a gravitation wave (GW) signal, thus reducing the detector sensitivity. In particular one important limitation will come from Brownian motion of the coated surface of the mirrors [5]. In order to reduce this contribution, the use of Laguerre-Gauss (LG) high order modes has been proposed [6]: the $LG_{3,3}$ beam will average the Brownian motion over a larger effective surface with respect to a fundamental Gaussian mode, resulting in a significant improvement in the detector sensitivity.

To use a $LG_{3,3}$ beam in gravitational wave detectors it is necessary to solve three main issues: generation of a pure mode; good matching of the mode with the resonant cavities of the interferometer; achievement of proper resonance conditions inside the cavities.

For what concerns the first issue, generation of a mode with a purity as high as 99% has been demonstrated [7,8]

using a linear mode cleaner. We are not addressing the $LG_{3,3}$ mode generation in this paper: we assume that high purity is achievable. We might note that the technique we propose in this paper can be used also to improve the filtering capabilities of linear mode cleaner cavities.

Recent work [9] showed that the matching on the resonant cavity is not a trivial problem. However, the use of adaptive optics techniques has already been shown as a viable solution to obtain matching as good as 99% in Advanced Detectors [10,11]. We will discuss the effect of residual mismatch in Sec. V, showing that the technique we are proposing is robust against it.

Finally, resonance of a $LG_{3,3}$ mode in cavities with spherical mirrors has already been demonstrated [8]. However, the $LG_{3,3}$ mode (called from now on the *fundamental mode*) is degenerate with nine other 9th order LG modes (modes $LG_{p,l}$ with $2p + |l| = 9$, called from now on *degenerate modes*). Any deviation of the mirror surface from the ideal one will introduce a coupling from the fundamental mode to the degenerate modes. This in turn will introduce additional losses inside the resonant cavity and it will create a significant amount of unwanted modes in reflection of the interferometer arm cavities [12,13]. These modes will be different in the two arm cavities and therefore will seriously limit the contrast defect of the

*gabriele.vajente@pi.infn.it

interferometer and as a consequence they will spoil the detector sensitivity.

For this reason the surface figure requirement for the mirrors to be used with a $LG_{3,3}$ input mode are very stringent [12], at the level of 0.01 nm root-mean-square (RMS), which is beyond present polishing and metrology capabilities. With the best available mirror quality, the beam reflected by a second generation GW detector Fabry-Perot cavity would only have a purity of the order of 90% [12]. The goal is to increase the purity to the 99.97% level that one would obtain, using the same maps, for a fundamental Gaussian mode in input [14].

In this paper we tackle the last issue, proposing a sensing and control technique to improve the resonance of $LG_{3,3}$ modes inside Fabry-Perot cavities, allowing a significant increase in the quality of the reflected beam and therefore making it possible to obtain a good interferometer contrast.

In [14] the use of a thermal correction pattern imaged onto the mirrors has been proposed as a viable technique to correct in-situ the mirror surface with great accuracy. The CHRAC system (Central Heating for Residual Aberration Correction) consists of an array of heating elements, each one with a size of the order of 1 cm. Each element's temperature can be controlled with high precision tuning of the driving current. An infrared (thermal) image of the array is then projected onto the mirror surface to be corrected, using an optical telescope. The resolution of the CHRAC system is set by the interplay between the size of the projected image of each element and the thermal diffusion length of the mirror. The paper [14] demonstrated the feasibility of applying a thermal correction pattern in order to reduce the degeneracy of high order modes in advanced detectors. It also showed that the same approach is applicable in the case of the $LG_{3,3}$ input mode. In both cases knowledge of the mirror surface map was assumed. This is a significant limitation in the case of the $LG_{3,3}$ mode since, as already pointed out, the level needed for surface accuracy is beyond present metrology capabilities. Moreover, additional deformations are expected due to stresses induced by the suspension system. Therefore it will not be possible to have reliable maps of the mirror surfaces to compute the optimal correction to be applied.

In this paper we are not addressing the technological aspects of the CHRAC system that were already discussed in [14]. We assume to have a *correction system* capable of projecting any desired heat pattern onto the mirror, with a maximum spatial frequency of the order of 1 cm^{-1} . Indeed, for what concerns this paper, the way the correction is applied is not important, provided it can be done in-situ. Therefore, other techniques, such as scanning CO_2 lasers [15], can be employed. We moreover assume that the correction map is reproduced perfectly. For what concerns the CHRAC system, it was shown in [14] that the error introduced by the correction system has a very small effect on the efficiency of the system. In addition, as described in

Sec. IV, we propose to implement an iterative loop that is capable of compensating for small residual errors in the correction pattern.

In this paper we propose and demonstrate with simulations [16] an adaptive optics sensing and control technique in which the surface correction map to be applied is computed without any *a priori* knowledge of the mirror maps, but using only information extracted from the amplitude image of the beam reflected by the cavity. We consider the application of this technique to a cavity with realistic mirror maps and show that it is possible to recover a very good purity of the $LG_{3,3}$ mode in reflection.

In Sec. II we show how to derive a small set of maps that form a basis for all the surface corrections to be applied to the mirrors that are relevant to reduce the coupling between the fundamental and the degenerate modes. In Sec. III we develop an image processing technique that allows us to extract a complete mode decomposition of the cavity reflection from just the amplitude image. In Sec. IV we show how to use this mode decomposition to implement the complete control system and to correct for any mirror surface defects. Finally, in Sec. V we discuss the robustness of the proposed algorithm against sensing errors.

II. MODE-GENERATING CORRECTION MAPS

The correction system will be composed of quite a large number of pixels ($N \sim 100$). The most general actuation scheme for the correction of one mirror could be to implement a search [17] over the N -dimensional space, trying to optimize a suitable merit function, like for example the purity of the cavity reflection in terms of the fundamental mode. However, the efficiency of this optimization, mainly in terms of time needed, depends strongly on the number of parameters involved. This consideration motivates the investigation of strategies to reduce the number of actuation parameters.

The goal of the correction is to minimize the amount of degenerate modes in reflection of the cavity, thus simultaneously improving the fundamental mode purity. We start the investigation by considering how these modes are created in reflection from a single mirror. More in detail, we ask ourselves what is the surface map needed to create a coupling from the fundamental mode to a $LG_{p,l}$ mode. More formally, in the short distance approximation [16], we describe the field reflected by a mirror by

$$\begin{aligned} E_r(x, y) &= \exp\left(-\frac{4i\pi}{\lambda}z(x, y)\right)LG_{3,3}(x, y) \\ &\simeq LG_{3,3}(x, y) + i\frac{4i\pi}{\lambda}z(x, y)LG_{3,3}(x, y), \quad (1) \end{aligned}$$

where z is the mirror map expressed as the surface displacement with respect to the ideal reference, λ is the laser wave-length and E_r is the reflected field. We have assumed the reflectivity of the mirror equal to one. All fields and the mirror map are functions of the transverse coordinates

(x, y) . The approximate equality in the above equation comes from the consideration that only small corrections of the mirror surfaces will be needed. We want to create a field composed of the fundamental mode plus a small contribution from another mode (we are clearly interested only in small values $|\alpha| \ll 1$):

$$E_g(x, y) = \text{LG}_{3,3}(x, y) + i\alpha \text{LG}_{p,l}(x, y), \quad (2)$$

where α is the spurious mode coefficient, which in the general case can be complex. The best mirror map $z(x, y)$ is then found by minimizing the mean square difference between the reflected and the target fields:

$$E[z] = \iint |E_g(x, y) - E_r(x, y)|^2 dx dy, \quad (3)$$

where the integration is carried out over the entire mirror surface. The minimum value of the error $E[z]$ can be found with standard variational techniques, solving the Euler-Lagrange equations associated with the above functional [18]:

$$z(x, y) = \frac{\lambda}{4\pi} \text{Arg} \left[1 + i\alpha^* \frac{\text{LG}_{p,l}^*(x, y)}{\text{LG}_{3,3}^*(x, y)} \right]. \quad (4)$$

The computation is described in the Appendix A 1. An example of the maps obtained with this formula is shown in Fig. 1. The problem with this solution comes from the presence of the $\text{LG}_{3,3}(x, y)$ function at the denominator, which introduces sharp features in the map that are not

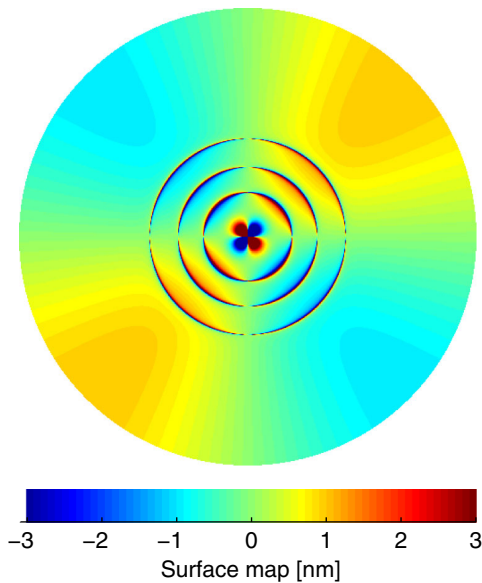


FIG. 1 (color online). Mirror surface map, computed analytically, that gives the best coupling from a $\text{LG}_{3,3}$ to a $\text{LG}_{4,1}$ mode. The coated mirror diameter considered here is 51 cm, which is that needed to have a cavity capable of sustaining a $\text{LG}_{3,3}$ mode with about 6 cm Gaussian radius with 1 ppm clipping losses (see also Sec. II). The color scale has been clipped to best show the map features.

realizable with the correction system, since they contain components at high spatial frequencies.

We therefore adopted a different approach, which allows us to retain control of the frequency content of the correction maps. Following the approach described in [13], we expand $z(x, y)$ in terms of Zernike polynomials Z_n^m [19]. As demonstrated in [13], we can restrict ourselves to using only the polynomials that satisfy the selection rule $m = |3 - l|$ where l is the azimuthal index of the target LG mode. For simplicity of notation, we list the Zernike polynomials up to a given order with a single index. Therefore the desired mirror map can be written as

$$z(x, y) = \sum_{i=1}^N p_i Z_i(x, y). \quad (5)$$

The error of Eq. (3) becomes a function of the Zernike coefficients:

$$E[p] = \iint \left| i\alpha \text{LG}_{p,l} + \frac{4\pi i}{\lambda} \sum_{i=1}^N p_i Z_i \text{LG}_{3,3} \right|^2 dx dy. \quad (6)$$

The coefficient vector $\mathbf{p} = (p_0, p_1, \dots, p_N)^T$ gives the optimal map for each mode that can be found by solving analytically the above least-square problem. The computation is detailed in the Appendix A 2, here we report the results:

$$\begin{aligned} \mathbf{p} &= -\mathbf{B}^{-1} \cdot \mathbf{A}, \\ A_k &= \iint (\alpha^* \text{LG}_{3,3} \text{LG}_{p,l}^* + \alpha \text{LG}_{3,3}^* \text{LG}_{p,l}) Z_k dx dy, \\ B_{i,j} &= \frac{8\pi}{\lambda} \iint |\text{LG}_{3,3}|^2 Z_i Z_j dx dy, \end{aligned} \quad (7)$$

where the vector \mathbf{A} and the matrix \mathbf{B} involved in the first equation are defined in the second and third equations. When the number of Zernike modes $N \rightarrow \infty$, the solution found with this technique approaches the one obtained with Eq. (4).

The choice of the maximum order of the Zernike polynomials gives us control over the maximum spatial frequency of the correction map. When implementing numerically the solution given by Eq. (7), some care is needed when inverting the matrix \mathbf{B} . Indeed, if the bare inverse is used, the maps that are found typically contain large corrections close to the edge of the mirrors. This is an undesirable feature, since we want to reduce as much as possible the amplitude of the correction. Moreover, the beam is mainly concentrated in the central part of the mirror, therefore the shape of the peripheral part of the mirror is less important. To better understand the origin of this large correction, the matrix \mathbf{B} can be described with a singular value decomposition (SVD) [[20], sec. 2.6].

In the general case, the smallest singular values correspond to correction modes that require very large amplitudes for almost no improvement of the merit function. In addition, in this particular case the smallest singular values

correspond also to correction modes that are mainly concentrated in the outer part of the mirror. Therefore if we compute the inverse of \mathbf{B} after truncating the decomposition to the modes with the largest singular values, we can restrict the correction to the central part of the mirror. Provided the truncation is not too extreme, the effect on the efficiency of the maps is negligible. In summary, by tuning the maximum order of the Zernike expansion and the threshold for SVD truncation we can control both the spatial frequency and the covered region of the correction. In this way it is possible to ensure that we obtain maps that can be implemented with the correction system.

We are interested in the set of maps that can couple the fundamental $\text{LG}_{3,3}$ mode to each of the nine degenerate modes. Since the LG modes are complex, the coefficient α of the target mode can have both real and imaginary components. Therefore, for each of the degenerate modes, two maps must be computed: one that generates the real part and another that generates the imaginary part. Therefore the algorithm produces in total 18 maps.

Since the criterion chosen to define an optimal map, given by Eq. (3), is related to the minimization of the mean square difference between the target field and that reflected by the mirror, the resulting set of maps is not completely diagonal in the basis of the ninth order LG modes: in other words the field reflected by one of the maps contains not only the desired ninth order mode, but also a small fraction of the other degenerate modes. Therefore we need to diagonalize the outcome of the previous computations. In this way we have a set of 18 *mode-creating maps* $\mathcal{M} = \{M_1, \dots, M_{18}\}$: the reflection of a $\text{LG}_{3,3}$ beam on a mirror with the map M_i will be composed of a $\text{LG}_{3,3}$ plus a contribution with coefficient α (real or imaginary, depending on the map chosen) of only one of the other degenerate modes $\text{LG}_{p,l}$. In other words, any arbitrary linear combination, with complex coefficient, of the degenerate modes can be obtained in reflection of a mirror with a surface map composed using only the maps in the set \mathcal{M} .

An example of the maps obtained using this procedure is shown in Fig. 2. We considered the application of this technique to the Fabry-Perot resonant cavity of a GW detector with the same geometry as Advanced Virgo [1]: the cavity length is of 3 km and the input and end mirror radii of curvature are respectively 1420 m and 1683 m. The Gaussian beam size corresponding to this geometry is of 48 mm on the input mirror and 59 mm on the end mirror. To reduce the clipping losses of a $\text{LG}_{3,3}$ beam below 1 ppm, the mirror diameter must be of about 52 cm. It would also have been possible to reduce the beam spot size in order to use more standard diameters of about 30 cm. However the core of the results shown in this paper would be unchanged.

The dependency of the maps \mathcal{M} on the maximum order of the Zernike polynomials involved in the optimization has been studied. It was found that the result is stable when the maximum order of the expansion is at least 24, for the

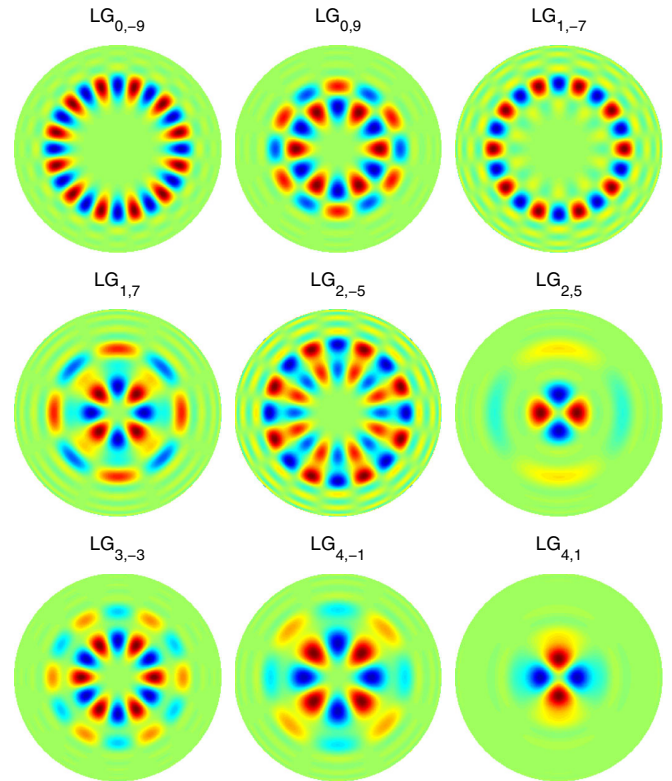


FIG. 2 (color online). Maps to generate ninth order LG modes in addition to the input $\text{LG}_{3,3}$. Only the maps that generate the mode with real coefficients are shown. The maps that generate those with imaginary coefficients are simply rotated by $\pi/4l$. These maps have been computed using parameters corresponding to an Advanced Virgo-like resonant cavity, see the main text for more details.

given beam and mirror parameters. The important properties of these maps, which is evident from the pictures, is that they do not contain high spatial frequencies or sharp features and they are concentrated near the center of the mirror. Therefore they are realizable with a thermal correction system such as the CHRAC.

The set \mathcal{M} of these 18 maps is complete, in the sense that given any real mirror surface map $z(x, y)$, one can always find a linear combination of the maps in \mathcal{M} that completely eliminates the coupling from the $\text{LG}_{3,3}$ mode to all the other degenerate ones. This statement has been checked in simulation with many randomly generated maps, with a procedure similar to the one explained in [14]: a correction map made of a linear combination of M_i is added to a mirror with a surface map z ; the coefficients c_i of the linear combination are optimized in order to minimize the power in the unwanted degenerate modes:

$$P[\mathbf{c}] = \sum_{n=1}^9 \left| \langle n | \frac{4\pi i}{\lambda} \left(z(x, y) + \sum_{i=1}^{18} c_i M_i(x, y) \right) | 0 \rangle \right|^2, \quad (8)$$

where we have used the bracket notation to indicate the projection into LG modes, enumerated with a single index

n , with 0 corresponding to the fundamental LG_{33} mode. The minimum of the above function can be computed analytically, considering the orthogonality properties of the maps

$$\langle n|M_i|0\rangle = a(\delta_{i,n} + i\delta_{i,9+n}), \quad (9)$$

where the set of maps is ordered as follows: first the nine maps generating the degenerate modes with real coefficients, then the nine maps generating the modes with imaginary coefficients. Here a is a normalization constant which depends on the amplitude of the maps. Equation (8) simplifies to

$$P[\mathbf{c}] \propto \sum_{n=1}^9 |\langle n|z|0\rangle + N(c_n + ic_{9+n})|^2 \quad (10)$$

that is minimum when all terms of the sum are simultaneously null:

$$c_n = -\frac{1}{N}\mathcal{R}(\langle n|z|0\rangle) \quad c_{9+n} = -\frac{1}{N}I(\langle n|z|0\rangle), \quad (11)$$

where we indicated with $\mathcal{R}(x)$ and $I(x)$ the real and imaginary part of the complex number x .

Clearly this procedure to find the correction map is viable in a resonant cavity only if perfect measurements of the mirror surface maps are known. It is therefore interesting to investigate the possibility of finding the correction coefficients without *a priori* knowledge of the map. As explained at the beginning of this section, one possibility would be to implement a search: the fact that we know all the maps that are relevant to remove the degenerate modes reduces the number of parameters to 18 per mirror. This is still a large number, but not untreatable with optimization techniques based for example on stochastic parallel gradient descent algorithms [17].

Moreover, the fact that the mirror surface features that are really relevant can be described in terms of a reduced number of maps can provide a method to better define the polishing requirements: instead of providing limits on the Zernike polynomial contents as done for example in [13], one could give limits in terms of the mode-generating maps \mathcal{M} .

III. MODE DECOMPOSITION OF CAVITY REFLECTION

As pointed out in the introduction, to properly operate a gravitational wave interferometric detector with a $LG_{3,3}$ mode in input, the cavities must be corrected in order to have the purest possible mode in reflection. In real detectors it is normally possible to operate the two cavities separately and easily acquire amplitude images of the reflected beams, using standard CCD cameras. The goal of this section is to demonstrate that it is possible to extract a complete field decomposition of the cavity reflection using only amplitude images. As will be shown in the

next section, this is enough to implement a feedback system to compute the optimal correction, without knowledge of the mirror surface maps.

Figure 3(a) shows a simulated image of the beam reflected by a Fabry-Perot cavity, taken at the surface of the input mirror. In this simulation the end mirror is perfect and the input mirror has a realistic surface map randomly generated, with a RMS deviation from the reference sphere of about 0.5 nm. The map, shown in Fig. 3(b), couples partially the fundamental $LG_{3,3}$ that is feeding the cavity into the other degenerate modes. The field has been computed using an optical simulation based on a FFT algorithm [16], using a square window of 0.5 m sampled with 256 points. The optical parameters of the cavity are those already described in the previous section. In the following we will refer to the simulation outcome as the *real beam image*, in contrast with the *fitted beam image* which is the result of the image processing algorithm we are going to describe.

Since the beam reflected by the cavity is mainly composed of a $LG_{3,3}$, it is possible to extract from the real

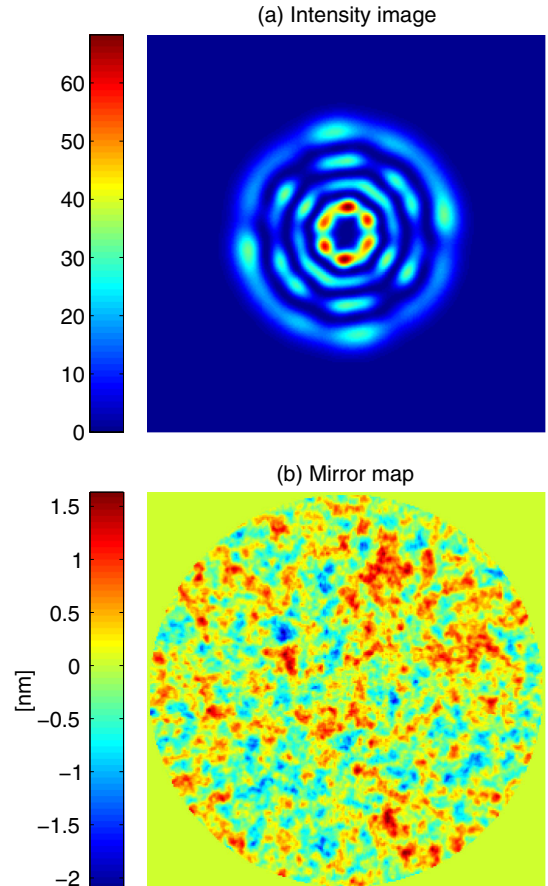


FIG. 3 (color online). Simulated power image (a) in reflection of a Fabry-Perot cavity with a perfect end mirror and an input mirror with a map randomly generated (b) that introduces some coupling from the fundamental mode to the other degenerate modes. The two images have the same transverse scale and the diameter of the mirror map is 51 cm.

power image the mode radius with a simple fit procedure which minimizes the mean square error between the image and the power profile of a pure fundamental mode, with unknown amplitude, width and center. The initial estimate of these parameters can be obtained using first and second order moments of the real image. The minimization is carried out using the Nelder-Mead simplex direct search algorithm [21].

The second step consists of fitting the real image with a complex linear combination of ninth order modes (denoted by Ψ_i with $i = 0 \dots 9$) computed with the beam parameters obtained with the above procedure. In other words we search for the best set of complex parameters α_i such that the power image

$$P(x, y; \alpha) = \left| \alpha_0 \Psi_0(x, y) + \sum_{i=1}^9 \alpha_i \Psi_i(x, y) \right|^2 \quad (12)$$

is the closest possible, again in a mean square sense, to the real beam image $I(x, y)$:

$$E[\alpha] = \iint |I(x, y) - P(x, y; \alpha)|^2 dx dy. \quad (13)$$

In Eq. (12) we separated the contribution coming from Ψ_0 which indicates the fundamental $\text{LG}_{3,3}$ mode, from the other ones. Indeed, in our application, the coefficient α_0 will be much larger than the other coefficients and will be the dominant contribution to the power image. The approximation $|\alpha_i| \ll |\alpha_0|$ can be included explicitly in the above minimization. In the general case it is possible to solve the least square problem using a numerical algorithm, such as the steepest descent method [[20], sec. 10].

It is clear from Eq. (12) that it will not be possible to completely reconstruct the mode coefficients: at least a global phase factor will remain unknown. In general one would expect to have many more uncertainties, since only the amplitude of the field is known. However, the numerical results, shown in Fig. 4, demonstrate that it is possible to fully reconstruct the complex amplitude of all coefficients, modulus the global phase. Figures 4(a) and 4(b) show that the amplitude is perfectly reconstructed. However, in Figs. 4(c) and 4(d) it is possible to see that also the phase is properly reconstructed over all the image, except for a tilt term which can be seen in Fig. 4(f). Finally, Fig. 5 compares the complex mode coefficients reconstructed using this algorithm with those obtained from a real decomposition which includes the beam phase information. The phase of both sets of coefficients has been normalized to that of the $\text{LG}_{3,3}$ to compensate for the unknown global phase. We see that there is very good agreement.

It is clearly not possible to use this procedure to extract any information on changes in the beam size and position, since these are free parameters in the fit procedure. Moreover, any tilt of the beam at the level of the camera is also not detectable, since it would add only a tilt term to the phase. However, these low order effects do not introduce any coupling between the ninth order LG modes, and therefore are not relevant to our objective.

The fact that such a complete knowledge of the beam modal decomposition is attainable can be surprising at first sight. Indeed for a beam composed of the most general mixture of LG modes, it is always possible to find a set of coefficients that properly fit the amplitude, but the solution is not unique. In our application, however, the fact that one

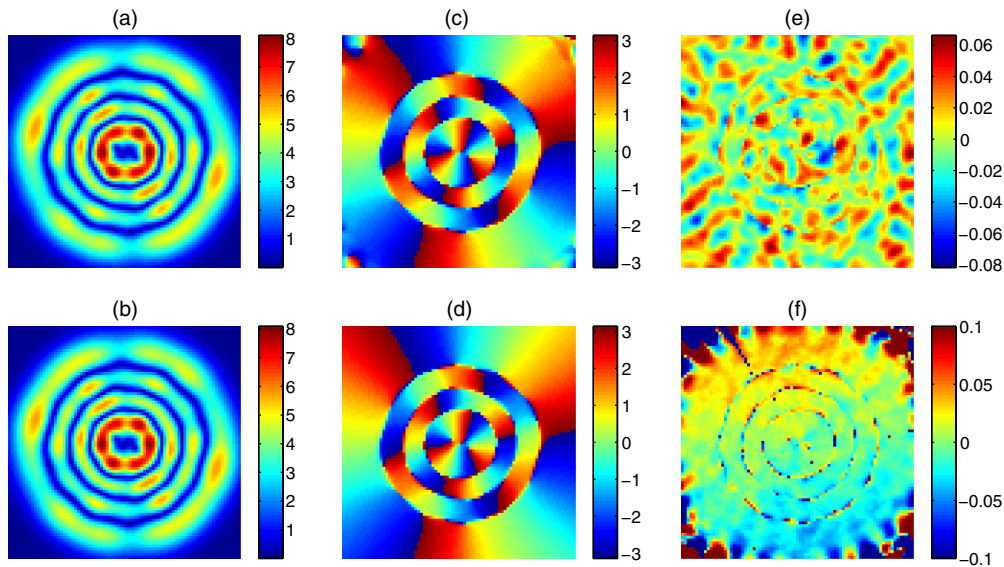


FIG. 4 (color online). Results of the reconstruction of the full field from intensity image only. (a) amplitude image of the real field; (b) amplitude image of the reconstructed field; (c) phase image of the real field; (d) phase image of the reconstructed field; (e) difference between the amplitude images; (f) difference between the phase images.

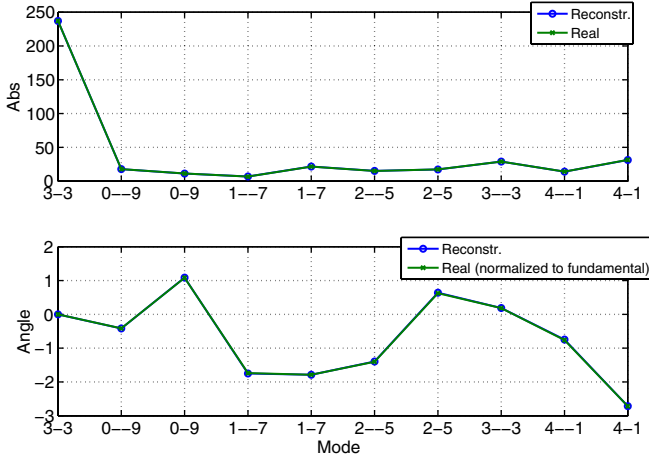


FIG. 5 (color online). Modal decomposition complex coefficient reconstructed from an intensity image, using the algorithm described in the text. They are compared with those obtained with a decomposition based on the full knowledge of the complex field.

of the modes is dominant, expressed by the approximation $|\alpha_i| \ll |\alpha_0|$, changes the nature of the set of Euler-Lagrange equations which determine the minimum of Eq. (13). In the general case they are of third order in all the coefficients. When the above approximation is introduced, these equations becomes linear in all coefficients α_i for $i \neq 0$ and retain their non-linear nature only for α_0 . The solution of this set of equations is therefore unique, except for the previously mentioned global phase, which can be fixed requiring α_0 to be real and positive. A complete proof of this statement is provided in the Appendix A 3, where the analytical solution of the minimization problem is given.

The coefficients found with this procedure are only first order approximations of the true ones. However, in our application, this approximation yields very good results, as shown in Fig. 5.

In conclusion, it is possible, starting from a pure intensity image of the cavity reflection, to reconstruct the mode content, in terms of the complex coefficients of all ninth order modes, taking as reference the phase of the injected $LG_{3,3}$ mode.

IV. CONTROL SYSTEM

The image processing algorithm described in the previous section allows to extract from a cavity reflected beam a set of error signals. These, together with the actuation described by the map set \mathcal{M} defined in Sec. II, provides all the ingredients needed to implement a complete adaptive optics system. The results shown in this section are based, as before, on a FFT simulation of a Fabry-Perot cavity, with an ideal end mirror and an input mirror with a randomly generated surface map. Each of the error signals e_i are given by the real or imaginary part of the coefficient

corresponding to that of the degenerate modes. These coefficients are extracted from the intensity image of the cavity reflection, taken at the input mirror surface. Since there are 9 modes which are degenerate with the $LG_{3,3}$, we have a set of 18 error signals.

The first step to building the control system consists of the calibration of the error signals. We select one of the maps M_i and we add it to the input mirror, multiplied by a scaling factor which is swept over a range that includes the optimal value, known from the results of Sec. II. All the error signals are computed for each point in the sweep. Figure 6(a) shows an example of the sweep of one map amplitude: it is clear that only one of the error signals is changing significantly, and is linearly proportional to the map amplitude. When we sweep the amplitude of the map that creates a given (real of imaginary) mode, we see that only the error signal corresponding to the same (real or imaginary) mode is changing. This perfect diagonalization is due to the fact that the beam image is taken exactly at the

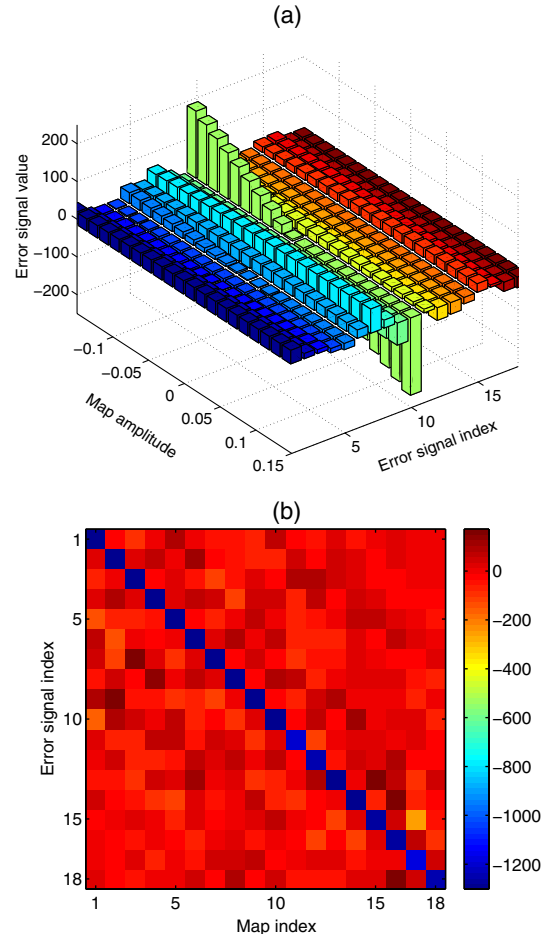


FIG. 6 (color online). (a) example of the dependence of all error signals on the amplitude of one selected map added to the input mirror of a Fabry-Perot cavity. (b) sensing matrix, composed of the slope of the linear dependence of all error signals on all map amplitudes.

input mirror. In the presence of an (ideal) imaging telescope, there will be a mixing between the error signals due to the induced change in Gouy phase.

The slope of the error signal variation as a function of the map amplitude can be extracted. When all maps have been added one by one, the set of slopes determines the sensing matrix S_{ij} which tells us the sensitivity of the i -th error signal to the j -th map amplitude. The result is shown in Fig. 6(b). We see that the diagonalization of the error signals is very good.

The adaptive optics control system is implemented as follows. The intensity image of the beam reflected from the

cavity is processed to extract the 18 error signals e_i . Each of these is the input of a simple integrator: its output is the amplitude c_i of the i th mode-generating map. The gain of the integrator is computed from the diagonal elements of the sensor matrix S_{ij} . The input mirror surface map is then modified with the addition of the linear combination of the mode-creating maps:

$$z'(x, y) = z(x, y) + \sum_{i=1}^{18} c_i M_i(x, y). \quad (14)$$

At this point we may assume that the correction system is capable of accurately reproducing any desired surface map correction.

The system described above was completely simulated, using several different randomly generated surface maps, applied to the input mirror of the same Fabry-Perot cavity considered above, with a finesse of 450. We consider here one map as an example of the typical results. Without any correction, the total round-trip losses in the cavity were about 15 ppm and the reflected beam was degraded such that only 92.9% of the power was in the $LG_{3,3}$ mode (see Fig. 7(a)). The control system is simulated by computing the correction in an iterative way: the steady state field reflected by the cavity is computed; the reflected beam image is processed to extract the error signals; the correction is computed and added to the input mirror; the cavity is simulated again and the entire procedure repeated. In about

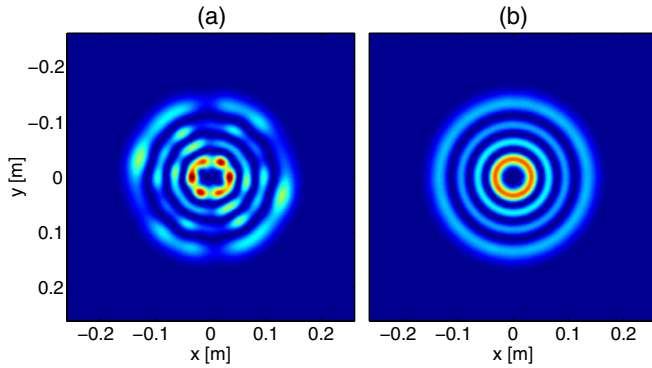


FIG. 7 (color online). (a) intensity image of the beam reflected by the cavity, without correction. (b) the same, with the correction computed by the adaptive optics control.

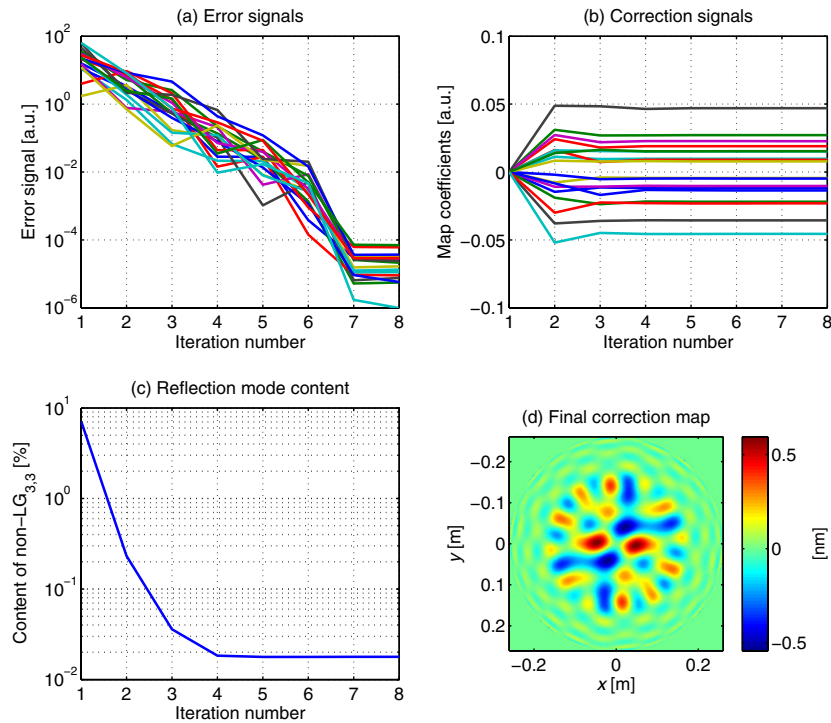


FIG. 8 (color online). Performances of the simulated adaptive optics control system. (a) evolution with the iteration number of the absolute values of the error signals; (b) evolution of the map coefficients; (c) evolution of the percentage of the reflected beam power which is not in the fundamental mode; (d) final correction map.

7 steps the correction converges to the final value (see Fig. 8). The cavity round-trip losses are essentially unchanged (17 ppm) but the purity of the reflected beam is largely improved: 99.98% is in the fundamental $LG_{3,3}$ mode (see Fig. 7(b)).

For simplicity, so far the simulation has been carried out keeping the end mirror of the cavity perfectly spherical. In the real world, both input and end mirrors will have maps with similar defects. The adaptive optics system described here is effective even in the case of two real mirrors. Moreover, it will not be necessary to actuate on both mirrors together, but one CHRAC system will be enough. Indeed, the two mirrors will create LG degenerate modes that will propagate inside the cavity and will be resonant. However, regardless of the origin of the modes, they will finally be present at the reflection of the cavity with some complex amplitudes. However, as shown in Sec. II, we are also able to generate each mode with arbitrary complex amplitude by acting on one single mirror. It will therefore be possible to cancel the unwanted modes from the cavity reflection using exactly the same compensation system described in the previous sections. This statement is confirmed by simulation. We added two different random maps to the input and end mirrors, such that the uncorrected cavity gives total round-trip losses of 50 ppm and a purity of the reflected beam of only 83%. In about 10 iterations, the adaptive optics system was able, acting only on the end mirror, to increase the purity of the reflected beam to 99.96%, without a significant change in the round trip losses (53 ppm).

The fact that it is enough to actuate only on one mirror is very important. As pointed out in [14], an actuation on the input mirror will introduce also a thermal lensing which, if not compensated by a thermal compensation system [22] could degrade the interferometer performance. It is therefore preferable to limit the actuation to the end mirror, where the additional thermal lensing can be neglected.

Finally, it might not be possible to perfectly reproduce the set of correction maps described in sec. II. It was shown in [14] that the CHRAC system is capable of a very good reproduction of the correction pattern. However, as long as each map is still capable of generating a not null amount of the desired degenerate mode, the iterative loop will correct for the imperfections, always converging to the point where all unwanted modes are canceled.

V. ROBUSTNESS AGAINST SENSING ERRORS

The simulation results presented so far assumed that it is possible to perfectly acquire the image of the reflected field. In real world applications there are several sources of image quality degradation. We briefly discuss in this section the effect of the main ones.

First of all, we must consider that the input beam waist size and position are not perfectly matched to those of the ideal cavity resonant mode. This mismatch introduces additional high order modes in reflection of the cavity.

However, the image processing technique proposed here is able to select only the ninth order modes and it is therefore insensitive to mismatch. To prove this statement, we simulated the effect of a mismatch of the input beam of 4%, meaning that in the case of a cavity with perfect mirrors only 96.29% of the reflected beam is in the cavity fundamental mode. The error signals obtained from the reflected beam are not affected by the mismatch and the iterative algorithm described here is able to converge to the same correction map as in the ideally matched case. The purity of the reflected beam is increased from 89.44% to 96.25%, with an efficiency comparable to that obtained with a perfectly matched beam.

In addition to a mismatch of the Gaussian mode, the input beam might not be pure, meaning that it can contain spurious ninth order modes in addition to the fundamental mode. The adaptive technique proposed here does not distinguish between the modes generated by the cavity and those already present in the input beam. The zero of the error signals will correspond to a reflected beam which contains the purest possible LG_{33} beam. The effect of the correction will therefore be to compensate for the unwanted modes in the input beam by modifying the mirror surfaces. This suggests also that the technique proposed here can be used to improve the quality of the beam generation.

In the simulation shown previously the image was taken exactly at the input mirror. In the real case however, the beam must propagate through additional optical elements before being imaged onto a camera. It is important to take care in designing the imaging system in order to avoid adding any aberrations to the field. To quantify the effect of such aberrations we simulated the propagation of the cavity reflected beam through a telescope similar to the one designed for the Advanced Virgo input system [1,23], composed of two parabolic mirrors and a meniscus lens. The main distortion is astigmatism: this can be handled in the algorithm that reconstructs the mode decomposition if the base is allowed to be scaled with respect to a possibly tilted axis. This is a simple extension of the fit in Eq. (12). The higher order aberrations introduce also a small coupling among the ninth order LG modes, resulting in an error of a few percent in the reconstructed coefficients. This effect is, for most part, compensated by the iterative approach described above. However, the correction which corresponds to the zero of all error signals is no longer equal to the ideal one. In the case of both input and end mirrors with surface maps, the iterative algorithm described above can be implemented reconstructing the error signal from the beam transmitted through a simulated output telescope. The correction obtained in this way, corresponding to the zero of all error signals, is slightly different from the ideal one, and is able to increase the reflected beam purity from 83% to only 99.65% instead of 99.96%. This indicates that the performance of the imaging system is important if we want to reach a very high purity of the beam.

We identified three possible ways to improve this situation. The most obvious one is of course to design the imaging optics in order to reduce the aberrations that create the largest deformations of the LG modes. This approach is outside the scope of this paper. The second possibility is to directly measure and subtract the aberrations induced by the imaging system. It is possible to measure the offsets added to the error signals, by sending a pure LG_{33} beam through the system and to the camera. This can be done, for example, by tilting the end mirror of the resonant cavity, in order to have only the prompt reflection from the input mirror. This mirror will still add its own aberrations to the LG_{33} input beam but, being outside of a resonant cavity, they will be much less important. Therefore we expect that the reflection of the input mirror alone will be a good purity LG_{33} mode and that any degenerate mode that would be detected at the level of the camera is introduced by the imaging system. We tested this idea in simulation: we reconstructed the field decomposition of the beam reflected by the input mirror alone and passing through the same telescope described above; the values were then subtracted from the error signals reconstructed during the iterative approach. In this way it was possible to completely remove the distortion and to recover the nominal 99.96% purity after correction.

Finally, in principle it would be possible to avoid using any imaging optical system, and look directly at the beam on the input mirror. Indeed the micro-roughness of the surface will produce a few ppm of scattered light that would provide enough power to image the beam directly. Clearly, this approach would be viable only in the case of a good homogeneity of the mirror scattering. We carried out several simulations adding a randomly generated power error on the beam images, with different amplitude and spatial frequencies. The results show that if the homogeneity of image power reconstruction is better than 5% it is possible to recover the nominal correction level of the beam. We did not consider the effect of point defects but we expect that these could be easily subtracted removing the corresponding pixel in the image. This idea of imaging directly the beam on the mirror is clearly appealing, but it needs more in depth studies.

VI. CONCLUSIONS

The main problem that will prevent the use of a $LG_{3,3}$ input beam in second and third generation interferometers is the poor contrast defect that will result from degenerate modes created by the imperfect mirror surfaces. We demonstrated with a detailed optical simulation that it is possible to implement a relatively simple adaptive optics system to correct for the mirror defects and recover a good purity of the mode reflected by the cavities and therefore a good contrast defect of the interferometer.

The system proposed here is rather simple and low cost. The actuation is performed using the CHRAC system, already described in detail in [14], which is capable of

correcting the mirror surface by projecting a thermal image with relatively high spatial resolution. The correction map needed to remove virtually all unwanted modes from the cavity reflection can be computed without any *a priori* knowledge of the mirror maps. Indeed, we showed that it is possible to extract the correction map using an image processing algorithm based only on an intensity image of the cavity reflection that can be obtained with CCD cameras.

Moreover, we showed that it is enough to apply the correction to only one of the two mirrors of the cavity. If the end mirror is chosen, the implementation of the proposed system will not add any burden to the existing thermal compensation systems.

In conclusion, the implementation of the adaptive optics system proposed here will allow the use of a $LG_{3,3}$ input mode in second generation interferometers with presently available mirror polishing and coating technology. If implemented in second generation detectors, this technique will allow a gain of a factor 1.6 [6] in the coating thermal noise and ultimately a significant improvement in the detector sensitivity.

ACKNOWLEDGMENTS

The research activity of one of the authors (G. V.) has been partially supported by Regione Toscana (Italy) through the program POR CreO FSE 2007-2013 of the European Community, within the Project No. 18113 (ISAV). The authors are also grateful to J. Marque (European Gravitational Observatory - Italy) for the many useful discussions on this paper.

APPENDIX: DETAILS OF THE COMPUTATIONS

This appendix gives more details on the computations that are needed to obtain the main results described in this article.

1. Analytical solution of mode-generating map

The goal is to find the function $z(x, y)$ describing a mirror surface that minimizes the error function defined by Eq. (3). It is possible to find the exact solution even without using the approximation $|z| \ll \lambda$. Indeed, using Eqs. (1) and (2) we get

$$E[z] = \iint |(1 - e^{-2ikz})\Psi_0 - i\alpha\Psi_1|^2 dx dy, \quad (A1)$$

where $k = \frac{2\pi}{\lambda}$ and for simplicity we set $\Psi_0 = LG_{3,3}$ and $\Psi_1 = LG_{p,l}$. Considering that the surface map is real and writing explicitly the absolute value we obtain

$$\begin{aligned} E[z] = & \iint [2|\Psi_0|^2 + e^{2ikz}(-|\Psi_0|^2 + i\alpha\Psi_0^*\Psi_1) \\ & + e^{-2ikz}(-|\Psi_0|^2 - i\alpha^*\Psi_0\Psi_1^*) \\ & - i\Psi_0^*\alpha\Psi_1 + i\Psi_0\alpha^*\Psi_1^* + |\alpha|^2|\Psi_1|^2] dx dy. \quad (A2) \end{aligned}$$

The extremal of this functional can be obtained solving the corresponding Euler-Lagrange equation, which takes a simple form:

$$0 = \frac{\partial E}{\partial z} = 2ike^{-2ikz}[e^{4ikz}(-|\Psi_0|^2 + i\alpha\Psi_0^*\Psi_1) + (-|\Psi_0|^2 - i\alpha^*\Psi_0\Psi_1^*)] \quad (\text{A3})$$

with the following solution:

$$e^{4ikz} = -\frac{|\Psi_0|^2 + i\alpha^*\Psi_1^*\Psi_0}{|\Psi_0|^2 - i\alpha\Psi_1^*\Psi_0}. \quad (\text{A4})$$

In this equation the numerator and the denominator of the fraction are complex conjugate. The value of z can be obtained therefore from twice the argument of the numerator:

$$\begin{aligned} \frac{8\pi}{\lambda}z &= 2\text{Arg}[|\Psi_0|^2 + i\alpha^*\Psi_1^*\Psi_0] \\ &= 2\text{Arg}\left[|\Psi_0|^2\left(1 + i\alpha^*\frac{\Psi_1^*}{\Psi_0^*}\right)\right] \\ &= 2\text{Arg}\left[1 + i\alpha^*\frac{\Psi_1^*}{\Psi_0^*}\right], \end{aligned} \quad (\text{A5})$$

which corresponds to Eq. (4).

2. Zernike polynomials expansion of mode-generating maps

In this case the mirror map is expressed as an expansion in terms of Zernike polynomials, using Eq. (5). Starting from Eq. (6) and using the same definition of Ψ_0 and Ψ_1 introduced in the previous section we get

$$E[p] = \iint \left| i\alpha\Psi_1 + 2ik\Psi_0 \sum_{i=1}^N p_i Z_i \right|^2 dx dy, \quad (\text{A6})$$

where we have this time used the approximation $|z| \ll \lambda$. For simplicity we call $\Delta\Psi = i\alpha\Psi_1$ the additional field that we want to create. The absolute value in the above integral can be expanded explicitly:

$$\begin{aligned} E[p] &= \iint \left[|\Delta\Psi|^2 + 2ik(\Psi_0\Delta\Psi^* - \Psi_0^*\Delta\Psi) \right. \\ &\quad \left. \times \sum_{i=1}^N p_i Z_i + 4k^2|\Psi_0|^2 \sum_{i,j=1}^N p_i p_j Z_i Z_j \right] dx dy. \end{aligned} \quad (\text{A7})$$

The optimal value for each Zernike coefficient can be found by setting to zero the corresponding partial derivative:

$$\begin{aligned} 0 = \frac{\partial E}{\partial p_k} &= \frac{4\pi i}{\lambda} \iint (\Psi_0\Delta\Psi^* - \Psi_0^*\Delta\Psi) Z_k dx dy \\ &\quad + \frac{32\pi^2}{\lambda^2} \sum_{i=1}^N p_i \iint |\Psi_0|^2 Z_k Z_i dx dy. \end{aligned} \quad (\text{A8})$$

The two terms in the right-hand side are respectively a vector A_k and the multiplication of a matrix B_{ik} with the vector of unknown coefficients p_i . This set of k equation is therefore a linear system with the solution given in Eq. (7).

3. Intensity image modal decomposition

Here we derive the analytical solution of the minimization problem defined by Eqs. (12) and (13):

$$E[\alpha] = \langle (I - P[\alpha])^2 \rangle, \quad (\text{A9})$$

where for simplicity we have denoted with angular brackets the integral over the entire x, y plane. We assume here that $|\alpha_i| \ll \alpha_0$ and that $\alpha_0 > 0$. At first order in the α_i the above equation becomes:

$$E[\alpha] = \left\langle \left[I - \alpha_0^2|\Psi_0|^2 - \alpha_0 \sum_{i=1}^9 (\alpha_i\Psi_0^*\Psi_i + \alpha_i^*\Psi_0\Psi_i^*) \right]^2 \right\rangle, \quad (\text{A10})$$

where Ψ_0 is the fundamental mode and Ψ_i are the degenerate modes. The optimal coefficients are found by setting to zero the partial derivative of e with respect to the coefficients α . We first consider the degenerate mode coefficients:

$$\begin{aligned} 0 = \frac{\partial E}{\partial \alpha_k} &= 2 \left\langle \left[I - \alpha_0^2|\Psi_0|^2 - \alpha_0 \sum_{i=1}^9 (\alpha_i\Psi_0^*\Psi_i + \alpha_i^*\Psi_0\Psi_i^*) \right] \right. \\ &\quad \left. \cdot (-\alpha_0\Psi_0^*\Psi_k) \right\rangle \end{aligned} \quad (\text{A11})$$

which, again at first order in the α_i gives the following equation

$$\begin{aligned} 0 &= -\alpha_0 \langle I\Psi_0^*\Psi_k \rangle + \alpha_0^3 \langle |\Psi_0|^2\Psi_0^*\Psi_k \rangle \\ &\quad + \alpha_0^2 \sum_{i=1}^9 [\alpha_i \langle (\Psi_0^*)^2\Psi_i\Psi_k \rangle + \alpha_i^* \langle |\Psi_0|^2\Psi_i^*\Psi_k \rangle]. \end{aligned} \quad (\text{A12})$$

With the following definitions:

$$a_k = \langle I\Psi_0^*\Psi_k \rangle, \quad (\text{A13})$$

$$b_k = \langle |\Psi_0|^2\Psi_0^*\Psi_k \rangle, \quad (\text{A14})$$

$$m_{ki} = \langle (\Psi_0^*)^2\Psi_i\Psi_k \rangle, \quad (\text{A15})$$

$$n_{ki} = \langle |\Psi_0|^2\Psi_i^*\Psi_k \rangle, \quad (\text{A16})$$

Eq. (A12) simplifies to

$$0 = -a_k + \alpha_0^2 b_k + \alpha_0 \sum_{i=1}^9 (m_{ki}\alpha_i + n_{ki}\alpha_i^*). \quad (\text{A17})$$

It is useful to decompose the coefficients in real and imaginary parts $\alpha_i = \rho_i + i\tau_i$. This allows us to rewrite the above equation in terms of real matrices and vectors. With the following definitions

$$\mathbf{R} = \begin{bmatrix} \rho \\ \tau \end{bmatrix} \quad (\text{A18})$$

$$\mathbf{A} = \begin{bmatrix} \mathcal{R}(\mathbf{a}) \\ I(\mathbf{a}) \end{bmatrix} \quad (\text{A19})$$

$$\mathbf{B} = \begin{bmatrix} \mathcal{R}(\mathbf{b}) \\ I(\mathbf{b}) \end{bmatrix} \quad (\text{A20})$$

$$\mathbf{M} = \begin{bmatrix} \mathcal{R}(\mathbf{m} + \mathbf{n}) & -I(\mathbf{m} - \mathbf{n}) \\ I(\mathbf{m} + \mathbf{n}) & I(\mathbf{m} - \mathbf{n}) \end{bmatrix} \quad (\text{A21})$$

Eq. (A17) further simplifies to

$$-\mathbf{A} + \alpha_0^2 \mathbf{B} + \alpha_0 \mathbf{M} \mathbf{R} = 0; \quad (\text{A22})$$

which is easily solved for the vector of field coefficients \mathbf{R} :

$$\mathbf{R} = -\alpha_0 \mathbf{M}^{-1} \left(\mathbf{B} - \frac{1}{\alpha_0^2} \mathbf{A} \right). \quad (\text{A23})$$

The value of α_0 can be found by solving the equation provided by the partial derivative of Eq. (A10) with respect to α_0 :

$$0 = -2\langle I|\Psi_0|^2 \rangle + 2\alpha_0^2 \langle |\Psi_0|^4 \rangle + 3\alpha_0 \sum (\alpha_i b_i + \alpha_i^* b_i^*) \quad (\text{A24})$$

with the same definition of b_i as in Eq. (A14). Using the definitions of Eqs. (A18) and (A20) we can write

$$\langle I|\Psi_0|^2 \rangle - \alpha_0^2 \langle |\Psi_0|^4 \rangle - 3\alpha_0 \mathbf{R}^T \mathbf{V} \mathbf{B} = 0 \quad (\text{A25})$$

with the additional definition of the matrix \mathcal{V} :

$$\mathcal{V} = \begin{bmatrix} \mathbf{1} & 0 \\ 0 & -\mathbf{1} \end{bmatrix}, \quad (\text{A26})$$

where $\mathbf{1}$ is the 9×9 unity matrix. The explicit solution for \mathbf{R} can be substituted from Eq. (A23). The equation for α_0 simplifies to a quadratic binomial:

$$0 = \langle I|\Psi_0|^2 \rangle - \alpha_0^2 \langle |\Psi_0|^4 \rangle + 3\alpha_0^2 \mathbf{B}^T \mathbf{V} \mathbf{M}^{-1} \mathbf{B} - 3\mathbf{B}^T \mathbf{V} \mathbf{M}^{-1} \mathbf{A} \quad (\text{A27})$$

with the unique solution, modulus a sign, given by

$$\alpha_0 = \sqrt{\frac{\langle I|\Psi_0|^2 \rangle - 3\mathbf{B}^T \mathbf{V} \mathbf{M}^{-1} \mathbf{A}}{\langle |\Psi_0|^4 \rangle - 3\mathbf{B}^T \mathbf{V} \mathbf{M}^{-1} \mathbf{B}}}. \quad (\text{A28})$$

This equation, together with (A23) uniquely determines all the coefficients α_0 and α_i .

-
- [1] Virgo Collaboration, Report No. VIR-027A-09, <https://tds.ego-gw.it/ql/?c=6589>.
- [2] G.M. Harry for the LIGO Scientific Collaboration, *Classical Quantum Gravity* **27**, 084006 (2010).
- [3] K. Kuroda, *Int. J. Mod. Phys. D* **20**, 1755 (2011).
- [4] The ET science team, Report No. ET-0106C-10, 2011, <https://tds.ego-gw.it/ql/?c=7954>.
- [5] S. Rowan, J. Hough, and D.R.M. Crooks, *Phys. Lett. A* **347**, 25 (2005).
- [6] B. Mours, E. Tournefier, and J.-Y. Vinet, *Classical Quantum Gravity* **23**, 5777 (2006).
- [7] M. Granata, C. Buy, R. Ward, and M. Barsuglia, *Phys. Rev. Lett.* **105**, 231102 (2010).
- [8] P. Fulda, K. Kokeyama, S. Chelkowski, and A. Freise, *Phys. Rev. D* **82**, 012002 (2010).
- [9] B. Sorazu *et al.*, *Classical Quantum Gravity* **30**, 035004 (2013).
- [10] M. Kasprzack, B. Canuel, F. Cavalier, R. Day, E. Genin, J. Marque, D. Sentenac, and G. Vajente, *Appl. Opt.* **52**, 2909 (2013).
- [11] B. Canuel, R. Day, E. Genin, P. La Penna, and J. Marque, *Classical Quantum Gravity* **29**, 085012 (2012).
- [12] T. Hong, J. Miller, H. Yamamoto, Y. Chen, and R. Adhikari, *Phys. Rev. D* **84**, 102001 (2011).
- [13] C. Bond, P. Fulda, L. Carbone, K. Kokeyama, and A. Freise, *Phys. Rev. D* **84**, 102002 (2011).
- [14] R. A. Day, G. Vajente, M. Kasprzack, and J. Marque, *Phys. Rev. D* **87**, 082003 (2013).
- [15] R. Lawrence, M. Zucker, P. Fritschel, P. Marfuta, and D. Shoemaker, *Classical Quantum Gravity* **19**, 1803 (2002).
- [16] J.-Y. Vinet, P. Hello, C.N. Man, and A. Brilllet, *J. Phys. I France* **2**, 1287 (1992).
- [17] M. A. Vorontsov, and V.P. Sivokon, *J. Opt. Soc. Am. A* **15**, 2745 (1998).
- [18] I. M. Gelfand, *Calculus of Variations* (Dover Publications, New York, 2000).
- [19] M. Born and E. Wolf, *Principles of Optics* (Cambridge University Press, Cambridge, England, 1999), 7th (expanded) ed.
- [20] W.H. Press *et al.*, *Numerical Recipes: The Art of Scientific Computing* (Cambridge University Press, Cambridge, England, 2007), 3rd ed.
- [21] J.C. Lagarias, J.A. Reeds, M.H. Wright, and P.E. Wright, *SIAM J. Optim.* **9**, 112 (1998).
- [22] A. Rocchi, E. Coccia, V. Fafone, V. Malvezzi, Y. Minkov, and L. Sperandio, *J. Phys. Conf. Ser.* **363**, 012016 (2012).
- [23] B. Canuel, E. Genin, G. Vajente, and J. Marque, *Opt. Express* **21**, 10546 (2013).